Computers & Geosciences 89 (2016) 239–251

Contents lists available at ScienceDirect

Computers & Geosciences

journal homepage: www.elsevier.com/locate/cageo

Research paper

Reconstruction of binary geological images using analytical edge and object models

Mohammad J. Abdollahifard*, Sadegh Ahmadi

Electrical Engineering Department, Tafresh University, Tafresh, Markazi Province, Iran

ARTICLE INFO

Article history:
Received 14 September 2015
Received in revised form
29 November 2015
Accepted 29 December 2015
Available online 4 January 2016

Keywords:
Prior model
Training image
Gradient descent
Inverse problems

ABSTRACT

Reconstruction of fields using partial measurements is of vital importance in different applications in geosciences. Solving such an ill-posed problem requires a well-chosen model. In recent years, training images (TI) are widely employed as strong prior models for solving these problems. However, in the absence of enough evidence it is difficult to find an adequate TI which is capable of describing the field behavior properly. In this paper a very simple and general model is introduced which is applicable to a fairly wide range of binary images without any modifications. The model is motivated by the fact that nearly all binary images are composed of simple linear edges in micro-scale. The analytic essence of this model allows us to formulate the template matching problem as a convex optimization problem having efficient and fast solutions. The model has the potential to incorporate the qualitative and quantitative information provided by geologists. The image reconstruction problem is also formulated as an optimization problem and solved using an iterative greedy approach. The proposed method is capable of recovering the image unknown values with accuracies about 90% given samples representing as few as 2% of the original image.

© 2015 Elsevier Ltd. All rights reserved.

1. Introduction

Characterization of environmental variables is accomplished using samples acquired by either in situ data-acquisition or remote sensing. Although with the development of complex acquisition methods the amount of data available for characterization of geological variables is becoming abundant, the complete sampling of a field is performed very rarely in practice due to financial and practical limitations. In other words there are always unsampled regions between acquired data which should be estimated using interpolation techniques.

Reconstruction of missing image data can be considered as an ill-posed inverse problem with many possible solutions. Therefore it is necessary to confine the solution space to geologically realistic patches using either regularization techniques (Lee and Seinfeld, 1987; Calderon et al., 2015) or probabilistic prior models. A multi-Gaussian distribution can be easily parameterized by mean and spatial covariance. Although mathematically convenient properties of multi-Gaussian distributions make them popular for modeling spatial variables (Chu et al., 1995; Li et al., 2003; Emery, 2007; Mariethoz et al., 2009; Abdollahifard and Faez, 2013b), their limited variability results in overly smoothed maps not consistent with realistic heterogeneities. Such methods are unable to reproduce the connectivity patterns appropriately for modeling flow and transport processes (Western et al., 2001; Knudby and Carrera, 2005; Bastante et al., 2008; Klise et al., 2009; Green et al., 2010). To alleviate this problem, some nonlinear and non-Gaussian high-order statistics models were developed based on spatial connectivity measures including spatial cumulants (Dimitrakopoulos et al., 2010) and copulas (Bárdossy and Li, 2008).

Object-based methods are able to produce realistic patterns with good spatial connectivity through defining basic shapes representing geobodies and placing them in the model domain based on a probability model (Deutsch and Tran, 2002; Allard et al., 2005; Keogh et al., 2007; Pyrcz et al., 2009; Michael et al., 2010). As an important advantage, object-based methods are able to control the parameters of geobodies (e.g. the channel width and orientation) to some extent. However, the conditioning to observed samples is usually achieved using a trial and error process resulting in a significant increase in computational complexity (Lantuéjoul, 2002; Allard et al., 2005).

The use of training images (TIs) has recently gained significant popularity for modeling environmental variability (Strebelle, 2002; Feyen and Caers, 2006; Zhang et al., 2006; Honarkhah and Caers, 2010; Mariethoz et al., 2010; Mariethoz and Renard, 2010; Abdollahifard and Faez, 2013a; Abdollahifard, 2015). The TI is an interesting tool for geologists allowing them to represent the desired geological concept in a direct manner (Feyen and Caers,

* Corresponding author.
E-mail address: mj.abdollahi@tafreshu.ac.ir (M.J. Abdollahifard).

http://dx.doi.org/10.1016/j.cageo.2015.12.018
0098-3004/© 2015 Elsevier Ltd. All rights reserved.

2006). To reconstruct an incomplete patch, multiple-point simulation (MPS) methods seek the TI to find a patch consistent with local samples. MPS methods are capable of producing realistic images conditioned to observed samples. The problem of finding a suitable patch among thousands of training patches (known as template matching problem) should be solved several times. As a result, MPS methods are CPU-intensive. Extensive effort was devoted to overcome this problem by using search trees or lists (Strebelle, 2002; Straubhaar et al., 2011), approximate gradient descent (Abdollahifard and Faez, 2013a), search space reduction (Abdollahifard, 2015), and training pattern clustering (Zhang et al., 2006; Honarkhah and Caers, 2010). Although the efforts have brought significant improvements in CPU-time, the approaches are still remarkably slower than their two-point predecessors because of their search-based nature.

The problem of selecting a proper training image is also a challenge in MPS approaches, especially when enough information is not available for such a decision. Selection of an inadequate TI may lead to realizations incompatible either with observed data or real field variations (Pyrcz et al., 2008; de Almeida, 2010). Even when the geological context is clear, constructing a complex 3D training image that adequately represents the complexity of geological structures requires lengthy computations (Mariethoz and Kelly, 2011).

Furthermore, unlike multi-Gaussian models or object-based models, it is not straightforward to parameterize the training images. In other words, the problem of TI selection is a discrete decision (either image A or B) and there is no parameter in a specific TI to be controlled continuously. Suzuki and Caers (2008) proposed a parameterization allowing several discrete choices of geological architectures within the prior. Another interesting TI parameterization is proposed by Mariethoz and Kelly (2011) by using small elementary training images as basic structural elements of the field and applying some parameterized transformations (e.g. rotation and affinity) on the lag vectors. Although the TIs selected are smaller than traditional ones, the additional continuous freedom degree (e.g. rotation) causes a remarkable increase in the search space.

The aim of this paper is, first, to introduce a single model capable of modeling a wide range of binary images and then, to exploit this model for reconstruction of missing image values. Consider the binary images depicted in Fig. 1(a)–(c). Although the images seem very different in macro-scale, their micro-scale building blocks are very similar as depicted in Fig. 1(d)–(f). In the selected scale, the patches have very simple structures and can be modeled effectively using one or a combination of two linear edges. This holds true for every binary geological image (either simpler or more complicated), if the proper patch size is considered.

In this paper an analytical model for linear edges is suggested with parameters controlling the edge orientation and sharpness. Thanks to the convenient mathematical properties of the suggested model, for any given incomplete patch (or a complete noisy patch) its corresponding match in the model space can be found in a few iterations using classical optimization techniques. This is in contrast to TI-based approaches whereby CPU-intensive exhaustive search is usually required to find a match in the TI. To achieve further flexibility, we have enriched the model space by allowing a combination of two linear edges capable of approximating narrow channels and nonlinear edges. Geologists' knowledge can also be incorporated by controlling the edge orientation range and setting relational constraints on two edges in

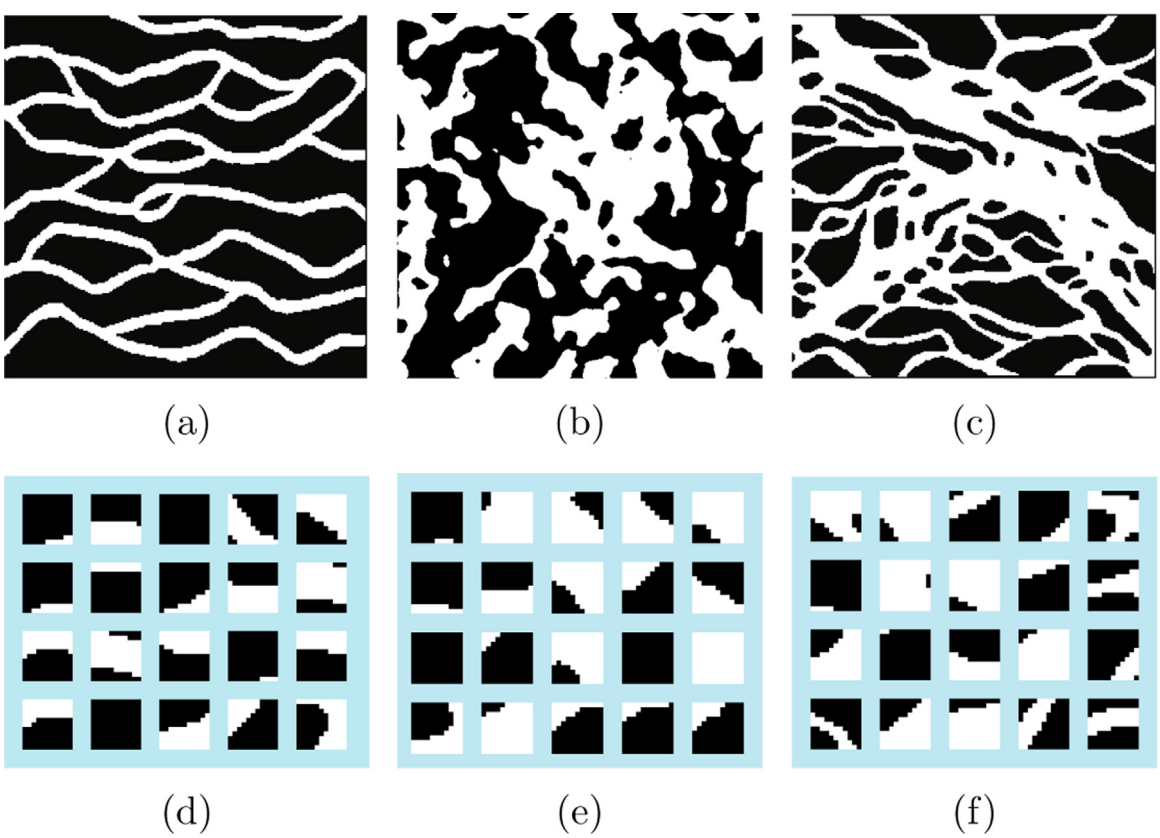

Fig. 1. Top row: three binary geological images (all images are obtained from the website of the book, Mariethoz and Caers, 2014). (a) A simplification of a channelized depositional system with white as sand and black as shale (Strebelle, 2002) of size 251×251, (b) a 245×245 image obtained from truncated Gaussian simulation, (c) a 243×243 image constructed based on a satellite image of the Ganges delta (Bangladesh), with soil properties classified as channel (white) and alluvial bars (black). Bottom row: 10×10 patches randomly extracted from binary images of top row.

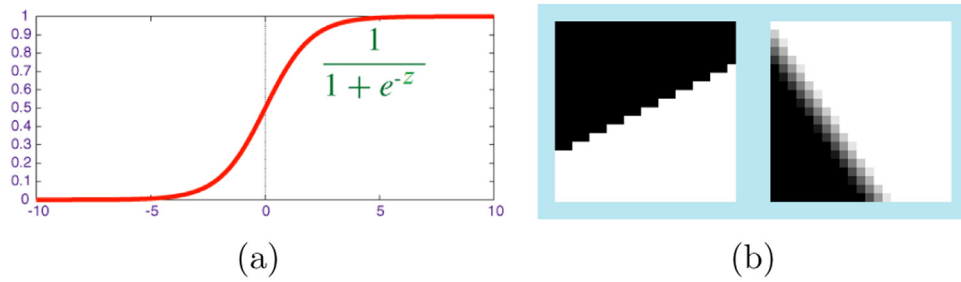

Fig. 2. (a) Sigmoid function and (b) two 21×21 patches synthesized using $f(\mathbf{x}; \mathbf{w})$ for $\mathbf{w} = [1, 1, 2]$ and $\mathbf{w} = [2, 0.3, -0.2]$ ($\mathbf{x} \in \{-10, -9, \ldots, 10\}^2$).

Fig. 3. Some templates synthesized using combinatorial model of Eq. (2) with different parameter settings.

the combinatorial model. In contrast to sequential simulation methods, in this paper the image content is retrieved using an iterative refinement method.

The paper is organized as follows. In Section 2 an overview of the proposed method is presented and the notations are introduced. In Section 3 two analytical models are introduced for image edges and objects. In Section 4 an image reconstruction algorithm is presented using the models. Section 5 is concerned with a gradient-descent algorithm for finding a match for a given patch in the model space. The results and comparisons are presented in Section 6.

2. Overview and notations

In this paper the goal is to reconstruct a binary two-dimensional image from a sparse set of samples extracted from random locations. The image is composed of M overlapping $n \times n$ patches denoted by $\tilde{\mathbf{p}}_i \in \mathcal{R}^{n \times n}$ $(i = 1, \ldots, M)$. The patches are vectorized for ease of mathematical manipulation and the vectorized form is denoted by $\mathbf{p}_i \in \mathcal{R}^N$ $(N = n^2)$. The ith patch contains a limited number of known values gathered in the vector $\mathbf{q}_i \in \mathcal{R}^{K_i}$ where $K_i \ll N$. In terms of mathematical notation, $\mathbf{q}_i$ can be shown as $\mathbf{q}_i = \mathbf{H}_i \mathbf{p}_i$ where $\mathbf{H}_i$ is a sampling matrix. Each row of $\mathbf{H}_i$ is responsible for extracting one sample. Therefore each row is composed of zeros in all indices except the sample location where the row element is equal to one.

Given $\mathbf{q}_i$, finding $\mathbf{p}_i$ is a severely ill-posed problem with many possible solutions. Therefore, it is necessary to confine the solution space by a patch model $\mathcal{M}$. Three models namely Unconstrained Linear Edge Model (ULEM), Unconstrained Combinatorial Model (UCM) and Constrained Combinatorial Model (CCM) are developed in this paper to confine the solution space. The reconstruction problem is formulated as a multi-objective optimization problem with two objectives for the patch: honoring the hard samples and fitting well in the model space.

The models are defined based on a parametric analytic function $f(\mathbf{x}; \mathbf{w})$ where $\mathbf{x} = [x_1, x_2]^T$ is a two-dimensional location vector and $\mathbf{w}$ is a vector containing the set of parameters. Assuming that n is an odd integer and $\mathbf{w}$ is a fixed vector, the function evaluated on all $\mathbf{x} \in \{-(n-1)/2, \ldots, (n-1)/2\}^2$ constitutes a $n \times n$ synthetic patch denoted by $\tilde{\mathbf{c}}(\mathbf{w}) \in \mathcal{R}^{n \times n}$. The vectorized counterpart is also denoted by $\mathbf{c}(\mathbf{w}) \in \mathcal{R}^N$. The set of all such patches for different parameter values constitute the model space. In this paper, the expanded form of the location vector is denoted by $\hat{\mathbf{x}} = [1, x_1, x_2]^T$.

Table 1
Image reconstruction algorithm.

Inputs: I_s, Parameters (n, N_{iters}, λ),
Outputs: I_r,
$I_r \leftarrow I_s$,
$I_t \leftarrow zeros(size(I_r))$,
for $iter = 1: N_{iters}$ **do**
  for $i = 1: M$ **do**
    $\mathbf{p}_i \leftarrow$ extract and vectorize ith patch from I_r,
    $\mathbf{q}_i \leftarrow$ extract the known values from the corresponding patch extracted from I_s,
    w-step: $\mathbf{c}(\mathbf{w}) \leftarrow$ find a match in the model space for $\mathbf{p}_i$,
    p-step: update $\mathbf{p}_i$ using Eq. (5),
    Insert $\mathbf{p}_i$ in the corresponding position in I_t, take average for overlapping values,
  end for
  $I_r \leftarrow \phi(I_t)$,
end for
Return I_r

3. Model

In order to solve an underdetermined inverse problem, a model is required to compensate the lack of sufficient observations. The model employed here is based on the key observation that, at a given scale, the image patches can be efficiently described using one or two linear edge models (see Fig. 1). In this section, a parametric model will be presented which confines the variability of patches to specific forms containing one or a combination of two linear edge models.

3.1. Unconstrained Linear Edge Model (ULEM)

In order to model the sharp transitions present in binary images an analytical edge model is introduced in this section. Assuming such a transition model for image patches, they will be reconstructed using a limited number of samples. The transition is modeled using a sigmoid function in the form:

$$g(z) = \frac{1}{1 + e^{-z}}. \tag{1}$$

As depicted in Fig. 2(a), the sigmoid function is zero for $z \ll 0$ and one for $z \gg 0$. The transition from zero to one occurs around $z = 0$. Suppose that $\mathbf{x} = [x_1, x_2]^T$ is a location vector in a 2D space and $\hat{\mathbf{x}} = [1, x_1, x_2]^T$. The edge model is considered as $f(\mathbf{x}; \mathbf{w}) = g(\mathbf{w}^T \hat{\mathbf{x}})$ where $\mathbf{w} = [w_0, w_1, w_2]^T$ is a weight vector. $f(\mathbf{x}; \mathbf{w})$ is composed of two regions with values around zero and one and the transition between the two regions occurs at a line identified by $w_0 + w_1 x_1 + w_2 x_2 = 0$ (see Fig. 2(b)). This simple analytical model can produce any linear edge with desired slope, x_2-intercept and sharpness. For binary images, however, we are concerned about the slope and the x_2-intercept of the edge not its sharpness.

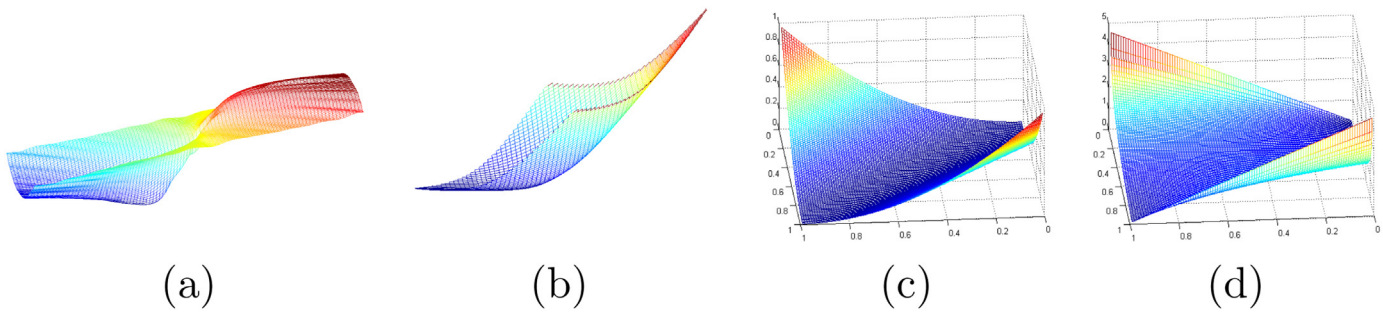

Fig. 4. For a synthetic noisy patch $\tilde{\mathbf{p}}$ produced using sigmoid function with known parameter setting, the distance $d(\tilde{\mathbf{p}}, f(\mathbf{x};\mathbf{w}))$ is evaluated for fixed w_0 and different values of w_1 and w_2 using Eqs. (6) and (9). The results are depicted in (a) and (b) respectively showing that the first objective function is non-convex and the second one is convex in terms of $\mathbf{w}$. (c) and (d) show $d_s(z_1, z_2) = (z_1 - z_2)^2$ and $d_{log}(z_1, z_2) = -z_1 \log(z_2) - (1 - z_1)\log(1 - z_2)$ for $z_1, z_2 \in (0, 1)$ (see the text for more information).

Fig. 5. Left pane: original synthetic noisy patch. Right pane: quantized form of $f(\mathbf{x};\mathbf{w})$ for $\mathbf{w}$ obtained from different iteration of gradient descent, from iteration 0 (random initialization) to iteration 4.

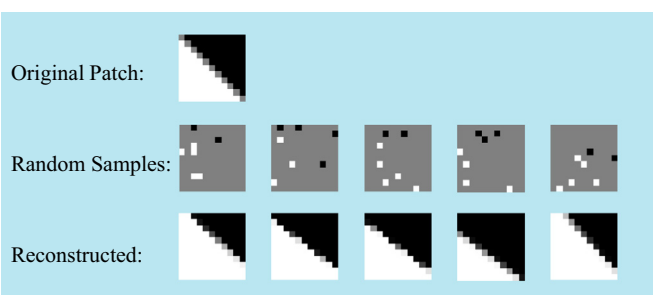

Fig. 6. Finding a match for a given patch using different sets of samples.

3.2. Combinatorial models

The limited variability of the above mentioned model causes difficulties for modeling narrow channels, nonlinear edges and jagged patterns. Different combinations of two sigmoid functions can be employed to enrich the model variability. Considering both pattern modeling capability and mathematical convenience, the following model can be constructed by superimposing two linear edge models:

$$f(\mathbf{x};\mathbf{w}) = f_1(\mathbf{x};\mathbf{w}_1) f_2(\mathbf{x};\mathbf{w}_2) = g(\mathbf{w}_1^T\hat{\mathbf{x}}) g(\mathbf{w}_2^T\hat{\mathbf{x}}) \tag{2}$$

where $\mathbf{w} = [\mathbf{w}_1^T, \mathbf{w}_2^T]^T$ is a parameter vector containing 6 parameters: $\mathbf{w}_1 = [w_{10}, w_{11}, w_{12}]^T$ and $\mathbf{w}_2 = [w_{20}, w_{21}, w_{22}]^T$. As illustrated in Fig. 3, this model is capable of synthesizing a broad variety of binary patterns containing narrow or thick channels, curved edges, and jag-like patterns. In the remainder of the paper this model is referred as Unconstrained Combinatorial Model (UCM). The Constrained Combinatorial Model (CCM) will be obtained by applying some constraints on UCM.

4. Image reconstruction

Image reconstruction is performed given the input hard samples along with the geologist's knowledge coded in the form of some constraints confining the model variability. Inspired by the work of Peyré (2009), in this paper the image reconstruction is formulated as an optimization problem with two objectives and a two-stage iterative optimization algorithm is proposed to handle the problem. For a specific patch, the objectives are to first maximize the fit to the conditioning data, and then to be confined in the model space as much as possible. This problem can be formulated as follows:

$$\mathbf{p}^* = \arg\min_{\mathbf{p}} \|\mathbf{q} - \mathbf{H}\mathbf{p}\|_2^2 \quad \text{subject to } \mathbf{p} \in \mathcal{M}, \tag{3}$$

where $\|.\|_2$ denotes the l_2 norm. Using Lagrange multipliers the constrained optimization problem can be converted to an unconstrained one as follows:

$$\{\mathbf{p}^*, \mathbf{w}^*\} = \arg\min_{\mathbf{p},\mathbf{w}} \{\|\mathbf{q} - \mathbf{H}\mathbf{p}\|_2^2 + \lambda\|\mathbf{p} - \mathbf{c}(\mathbf{w})\|_2^2\}, \tag{4}$$

where λ controls the relative importance of the two objectives. $\mathbf{c}(\mathbf{w})$ is a vectorized form of a $n \times n$ patch obtained from the model $f(\mathbf{x};\mathbf{w})$ for all $x \in \Omega = \{-(n-1)/2, \ldots, (n-1)/2\}^2$.

A greedy optimization algorithm can be employed to solve this problem whereby in the first step (w-step) $\mathbf{w}$ is computed by fixing $\mathbf{p}$, and in the second step (p-step) the problem is solved with respect to $\mathbf{p}$ assuming fixed $\mathbf{w}$. Interestingly, the above-mentioned objective function is quadratic in terms of $\mathbf{p}$. Therefore assuming constant $\mathbf{w}$, the optimum value for $\mathbf{p}$ can easily be found in closed form as follows:

$$\mathbf{p}^* = \left(\mathbf{H}^T\mathbf{H} + \lambda\mathbf{I}\right)^{-1}(\mathbf{H}^T\mathbf{q} + \lambda\mathbf{c}(\mathbf{w}^*)). \tag{5}$$

On the other hand, for fixed $\mathbf{p}$ the first term of the objective function reduces to a constant. Therefore, the optimum vector $\mathbf{w}$ is the one which minimizes the distance $d(\mathbf{p}^*, \mathbf{c}(\mathbf{w})) = \|\mathbf{p}^* - \mathbf{c}(\mathbf{w})\|_2$. In other words, in the w-step the nearest patch in the model space, $\mathcal{M}$, to the given patch $\mathbf{p}^*$ (or the projection of $\mathbf{p}^*$ on $\mathcal{M}$) should be determined.

The reconstruction algorithm is summarized in Table 1. I_s denotes the grid associated to the field of interest, which has values at the sampling locations and is unknown at other places. I_r denotes the reconstructed binary image. $\phi(\cdot)$ is a binary thresholding function applied to all pixels of the temporary variable I_t:

$$\phi(c) = \begin{cases} 0: c \le 0.5 \\ 1: c > 0.5 \end{cases}.$$

It should be noted that since the image values are updated at once (line 14 of Table 1), the algorithm is insensitive to the scanning

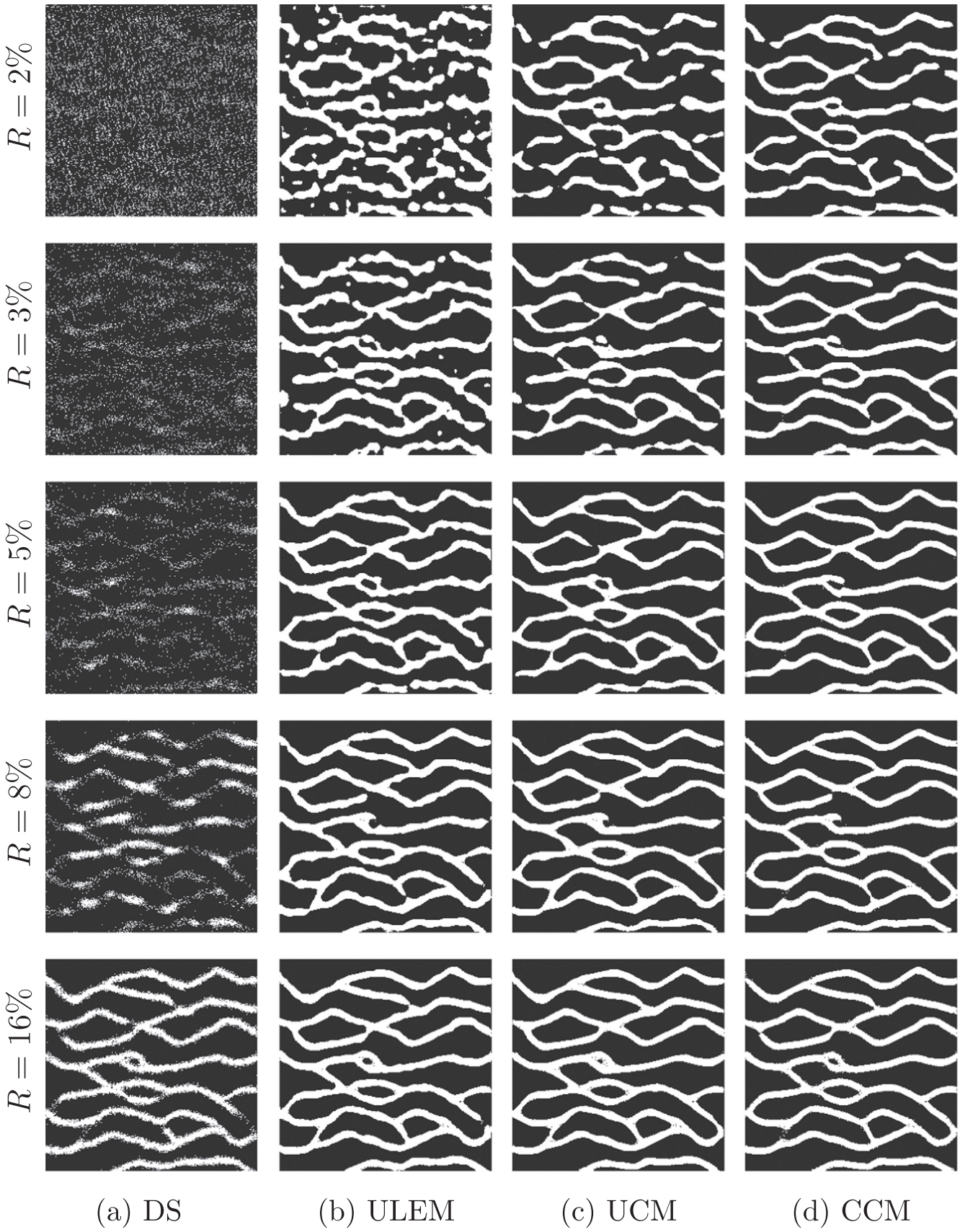

Fig. 7. Reconstruction of incomplete images sampled at different rates R=2%, 3%, 5%, 8% and 16% using DS (Mariethoz and Renard, 2010) and the proposed method with different models ULEM, UCM, and CCM. The tests are performed on randomly distributed samples extracted from Fig. 1(a).

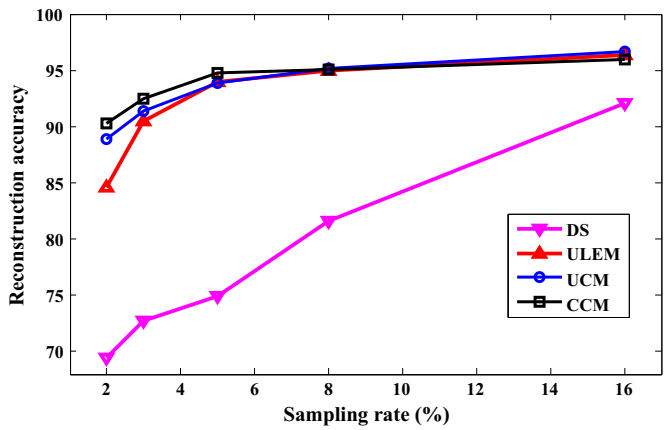

Fig. 8. Reconstruction accuracies for images depicted in Fig. 7.

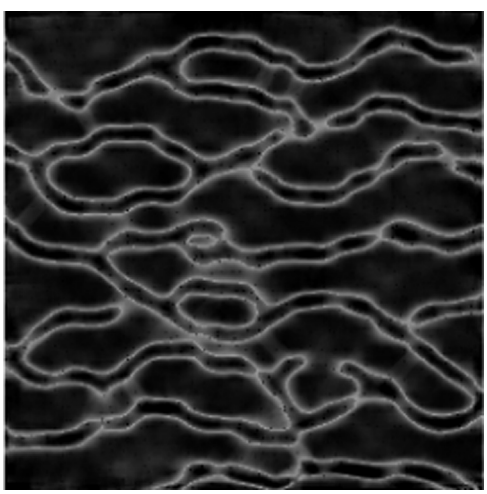

Fig. 9. Uncertainty map $U = |I_r - I_s|$ for CCM model with R=2% and n=21.

path. Therefore, a fixed raster path from top-left corner to the bottom-right corner of the image is considered in the algorithm. Furthermore, increasing the overlap between subsequent patches increases the reconstruction accuracy. Then, the algorithm is implemented with maximum possible overlap between subsequent patches. Hence, the window of a new patch is obtained by shifting the previous window by only one pixel.

5. Finding the match in the model space (w-step).

In this section the goal is to find a match in the model space $\mathcal{M}$ for a given patch $\mathbf{p}$. This problem is formulated using gradient-descent optimization for ULEM and UCM.

5.1. Linear edge model

Minimizing the distance between $\mathbf{p}$ and $\mathbf{c}(\mathbf{w})$ is equivalent to minimizing the distance between the matrix counterparts $\tilde{\mathbf{p}}$ and $f(\mathbf{x};\mathbf{w})$ over the grid Ω where Ω may be defined as the full grid $\{-(n-1)/2, \ldots, (n-1)/2\}^2$ or any subset of it:

$$d(\mathbf{p}, \mathbf{c}(\mathbf{w})) = d(\tilde{\mathbf{p}}, f(\mathbf{x};\mathbf{w})) = \sum_{x\in\Omega} (\tilde{\mathbf{p}}(\mathbf{x}) - f(\mathbf{x};\mathbf{w}))^2. \tag{6}$$

Note that the origin is assumed to be placed at the center of the patch. Assuming linear edge model, taking gradient with respect to the parameters $\mathbf{w}$ leads to:

$$\nabla_{\mathbf{w}}\, d = \frac{2}{|\Omega|} \sum_{x\in\Omega} \{(\tilde{\mathbf{p}}(\mathbf{x}) - f(\mathbf{x};\mathbf{w}))(f(\mathbf{x};\mathbf{w}) - 1) f(\mathbf{x};\mathbf{w})\hat{\mathbf{x}}\}, \tag{7}$$

where $|\Omega|$ indicates the number of the members of Ω. Using the gradient vector, the parameters can be updated using gradient-descent as follows:

$$\mathbf{w}^{t+1} = \mathbf{w}^t - \eta \nabla_{\mathbf{w}}\, d, \tag{8}$$

where η is a constant which controls the step size of gradient-descent algorithm.

Unfortunately, the objective function of Eq. (6) is non-convex in terms of $\mathbf{w}$. For a synthetic noisy patch $\mathbf{p}$ produced using sigmoid function with known parameters, the function evaluated for different values of w_1 and w_2 is depicted in Fig. 4(a) by fixing w_0 to its true value. From the figure one can verify that the function has small gradient in much of its support, even far from the optimum point. As a result, the gradient descent approach to the optimum is typically very slow, requiring numerous iterations. Furthermore, non-convex functions are likely to have local minima where gradient descent is prone to be trapped.

Such a problem was previously posed in machine learning literature where approximate solutions exist (Bishop, 2006). Inspired by the idea used for classification problems, we suggest to replace the squared distance $d_s(z_1, z_2) = (z_1 - z_2)^2$ with a logarithmic distance in the form $d_{log}(z_1, z_2) = -z_1 \log(z_2) - (1 - z_1)\log(1 - z_2)$ for $z_1, z_2 \in (0, 1)$. As depicted in Fig. 4(c) and (d), the distances d_s and d_{log} have similar behavior for $z_1, z_2 \in (0, 1)$. Based on this, the objective function of Eq. (6) is modified as follows:

$$d(\tilde{\mathbf{p}}, f(\mathbf{x};\mathbf{w})) = -\sum_{x\in\Omega} \left\{ \tilde{\mathbf{p}}(\mathbf{x}) \log(f(\mathbf{x};\mathbf{w})) + (1 - \tilde{\mathbf{p}}(\mathbf{x})) \log\big(1 - f(\mathbf{x};\mathbf{w})\big) \right\}. \tag{9}$$

Taking gradient with respect to $\mathbf{w}$ results in

$$\nabla_{\mathbf{w}}\, d = \frac{1}{|\Omega|} \sum_{x\in\Omega} \left\{ \big(f(\mathbf{x};\mathbf{w}) - \tilde{\mathbf{p}}(\mathbf{x})\big)\hat{\mathbf{x}} \right\}. \tag{10}$$

Analyzing the Hessian matrix it can be verified that the modified objective function is convex in terms of $\mathbf{w}$. For illustration, the same patch employed previously to produce Fig. 4(a) is used for evaluation of the new objective function of Eq. (9) and the result is depicted in Fig. 4(b). The convex behavior of the modified objective function makes gradient descent very efficient in finding the optimum.

For a given synthetic noisy patch $\tilde{\mathbf{p}}$ shown in the left pane of Fig. 5, the results produced with parameters of different iterations of gradient descent algorithm is depicted in the right pane ($\tilde{\mathbf{p}}$ is a 11×11 patch). It is worth indicating that, TI-based exhaustive search methods require at least 540 comparisons to solve such a template matching problem assuming 36 discrete choices for angle and 15 ($= \lfloor 11\sqrt{2} \rfloor$) choices for displacement.

The method is also applicable using incomplete sets of samples. Fig. 6 shows the reconstruction results of the method for a patch using just 5% of its samples extracted randomly. Interestingly, in all cases the produced results are close to the original patch.

5.2. Combinatorial model

The w-step for the combinatorial model can be carried out by minimizing the function (9) where f is defined in Eq. (2). The gradient-descent approach of Eq. (8) can be employed to solve this optimization problem. The gradient of d with respect to $\mathbf{w}$ can

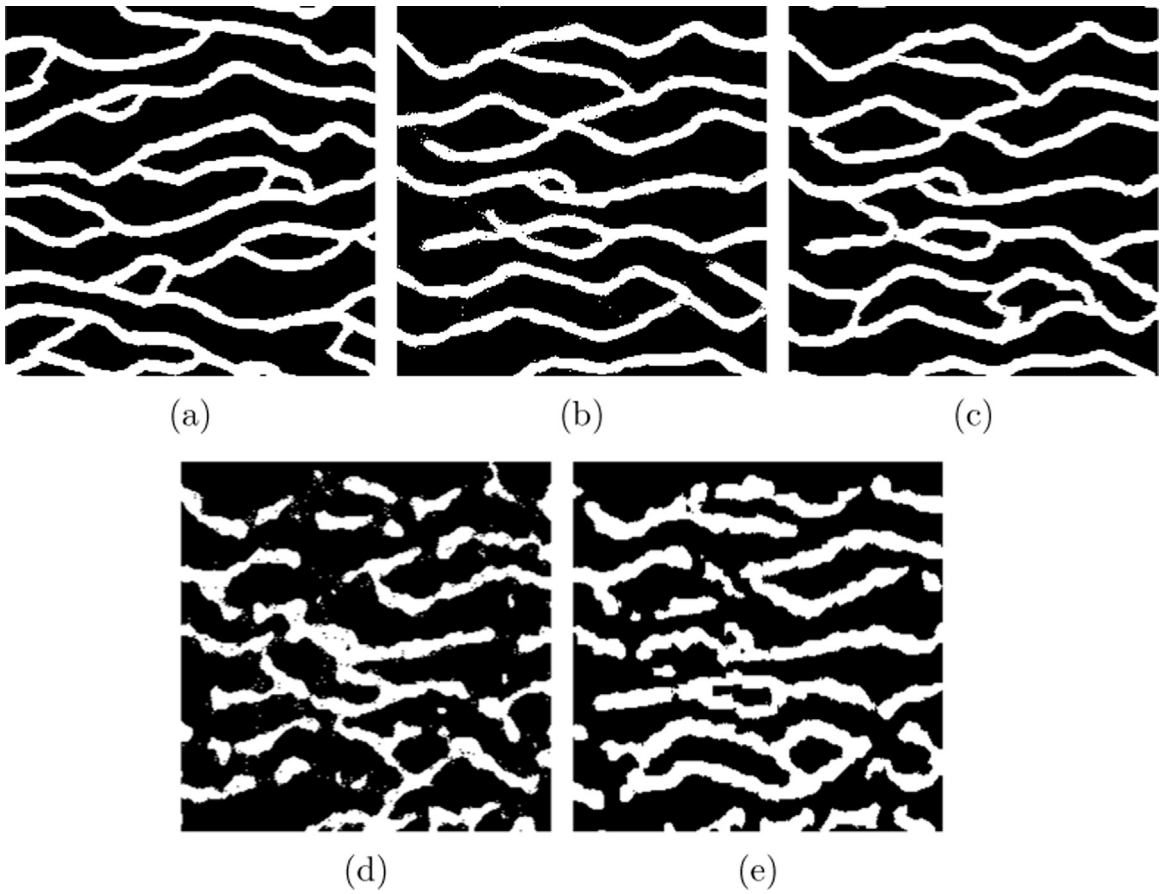

Fig. 10. Reconstruction of an incomplete image sampled at 3% rate using ordinary DS (Mariethoz et al., 2010) and SIMPAT (Arpat and Caers, 2007). (a) A representative image used as TI. (b) and (c) the results of DS and SIMPAT when using the appropriate TI of (a). The reconstruction accuracy is 92.25% and 90.13% respectively. (d) and (e) the results of DS and SIMPAT when using the inadequate TI of Fig. 1(b). The reconstruction accuracy is 84.80% and 84.93% respectively.

easily be obtained based on the partial derivatives given below:

$$\frac{\partial d}{\partial w_{ij}} = \sum_{\mathbf{x}\in\Omega} \left\{ \hat{\mathbf{x}}_j (1 - f_i(\mathbf{x};\, \mathbf{w}_i)) \left\{ \frac{f(\mathbf{x};\, \mathbf{w}) - \tilde{\mathbf{p}}(\mathbf{x})}{1 - f(\mathbf{x};\, \mathbf{w})} \right\} \right\}, \tag{11}$$

where $i \in \{1, 2\}$ and $j \in \{0, 1, 2\}$.

5.3. Constrained models

As indicated before, it is difficult to incorporate the qualitative and quantitative information provided by the geologists in the training images (TIs) in multiple-point statistics approaches. For example, if a geologist believes that a specific field is composed of a number of channels with a specific width ω, this information could be incorporated in a relatively large TI composed of a number of channels with different orientations. Fig. 1(a) can be considered as a subset of such an image which needs to be enriched by incorporating remaining orientations in order to represent the geologist's conceptual view. In order to add an additional degree of freedom, the TI needs to be enlarged several times. For example consider the case where the geologist is uncertain about the channel width and suggests an interval of $[\omega_1, \omega_2]$ for this parameter. Handling such a large TI requires excessive computational effort.

The geologist viewpoints can be incorporated in our approach by applying appropriate constraints to the solution space of the optimization problem. One way to solve a constrained optimization problem is first to ignore the constraint and find a solution to the unconstrained problem, and then to apply the constraint to the solution obtained from unconstrained optimization. In other words, the final solution is considered as the nearest point to the unconstrained optimization solution located in the allowed space. For example, this strategy can be incorporated in the combinatorial model by enforcing the two edges (sigmoids) to be parallel with a fixed distance of ω.

6. Results and comparisons

This section is concerned with the evaluation of the proposed method on different binary fields. Here, our method is compared with Direct Sampling (DS) which is a training-image based method (Mariethoz et al., 2010). Note that the proposed method does not exploit any additional data (like training images). For a fair comparison, our method is compared with a modified version of DS which uses the conditioning data itself as the training dataset, instead of exploiting a separate training image (Mariethoz and Renard, 2010).[1] This method completes an incomplete grid by scanning the grid in a random order. For each unknown value in the grid, a data-event containing n_{DS} known neighbors is extracted around it within a radius of r. Then, the data-event is compared with the corresponding neighbors of the known grid values to find an acceptable match. Next, the central value is copied from the found match to the query point. This process is repeated for all unknown pixels until the grid is completed. This is clearly a time-consuming method because it requires solving numerous

[1] The ordinary DS code is downloaded from http://www.minds.ch/gm and slightly modified to conform to the algorithm of Mariethoz and Renard (2010).

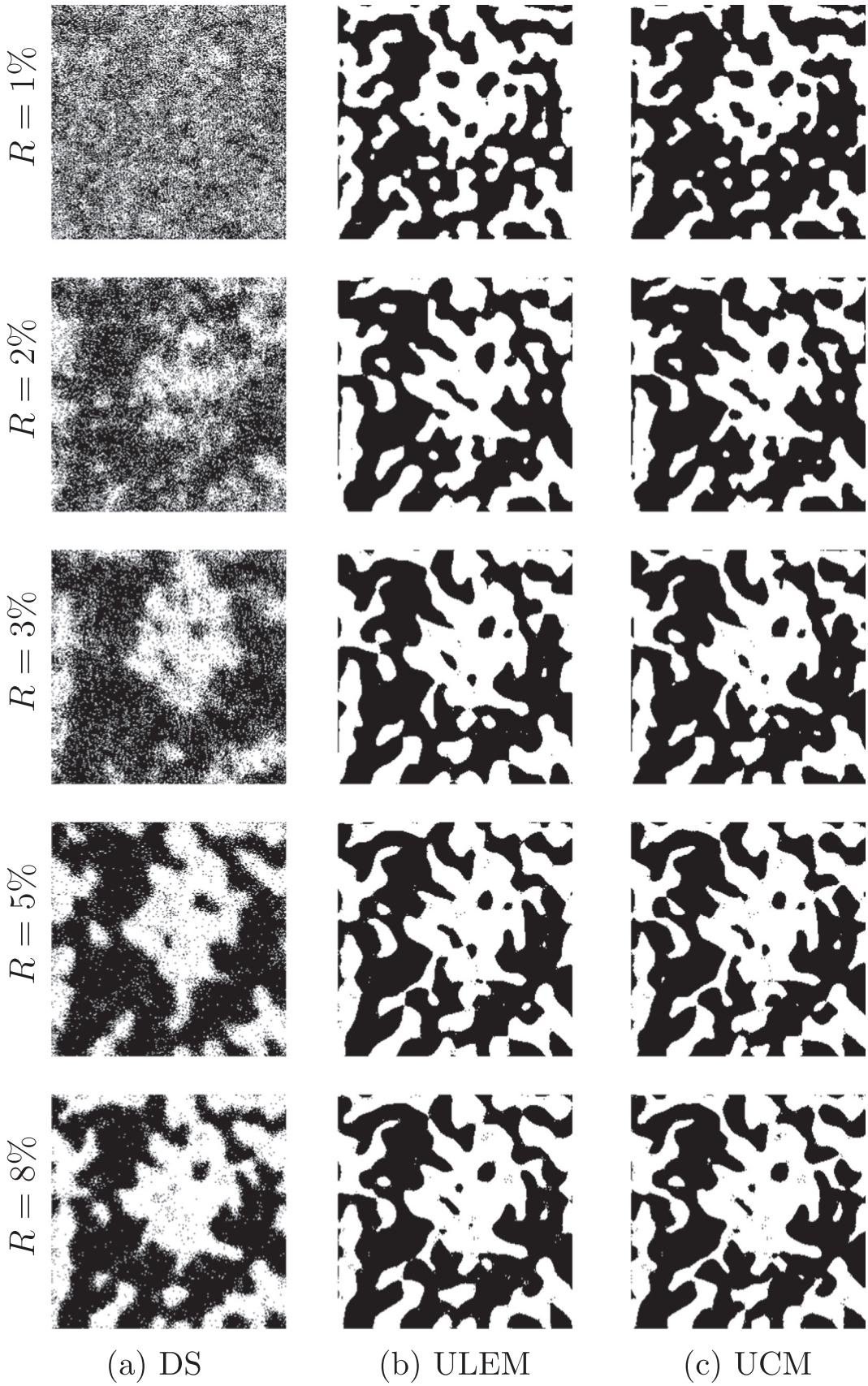

Fig. 11. Reconstruction of incomplete images sampled at different rates R=2%, 3%, 5%, 8% and 16% using DS (Mariethoz and Renard, 2010) and the proposed method with models ULEM and UCM. The tests are performed on randomly distributed samples extracted from Fig. 1(b).

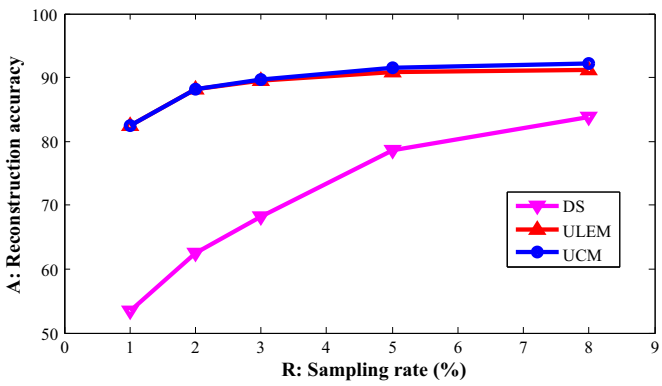

Fig. 12. Reconstruction accuracies for images depicted in Fig. 11.

exhaustive search problems. To alleviate this problem the authors suggest to search a fraction f of the image ($0 < f \leq 1$). However, to achieve acceptable results f is set to 1 in all of our tests. Furthermore, n_{DS} and r are set to 50 and 20 respectively.

The proposed method is implemented using three different models at its core: ULEM, UCM and CCM. There are a number of parameters in the proposed algorithm which can be adjusted by the user, namely N_{iters}, n, and λ in the main algorithm and η in gradient descent optimization. Fortunately, for most of the parameters a certain setting works quite well for different sampling rates in different images. In all tests we set $N_{iters} = 1$, $\lambda = 1$, and $\eta = 15$. As will be discussed later in more detail, the combinatorial model allows larger patch sizes.

The first experiment is carried out on the channelized image of Fig. 1(a) as the original image. The original image is sampled at randomly distributed locations with the sampling rate of R (%) to form an incomplete image I_s. Then different methods are employed to reconstruct the image using I_s. The patch size is set to 13×13 for ULEM and 21×21 for combinatorial models. The results of DS are compared with our results in Fig. 7 for sampling rates $R = 2\%$, 3%, 5%, 8%, and 16%. Given the original image I_o and the reconstructed image I_r, the reconstruction accuracy is defined as follows:

$$A = \left(1 - \frac{1}{N_I} \sum_{(x_1,x_2)\in\Lambda} |I_o(x_1, x_2) - I_r(x_1, x_2)|\right) \times 100, \tag{12}$$

where N_I denotes the number of pixels of I_o and Λ denotes the set of all positions at which I_o is defined. The accuracies obtained using Eq. (12) are reported in Fig. 8.

Fig. 7 (d) depicts the results of our method using CCM, where the constraint is applied by forcing the channel width to 8 pixels. For high sampling rates, all models perform equivalently well. However, at lower sampling rates, which are of particular interest in practice, the combinatorial models outperform the ULEM. Specifically, CCM provides significantly better results for 2% and 3% sampling rates from both quantitative and qualitative viewpoints.

DS provides poor performance in low sampling rates. The reason lies in the fact that DS does not exploit any model in the reconstruction process and relies only on conditioning data. The very simple model employed in this paper, which encourages step-like transitions between regions, makes it possible to achieve higher reconstruction accuracy. For example, the result obtained using CCM for 3% sampling is comparable to the one obtained using DS for 16% sampling. In other words, the proposed method makes it possible to achieve a certain level of accuracy using only one-fifth of the samples required by DS. This leads to a significant reduction in the sampling cost.

One may be concerned with the uncertainty associated with the estimations. The uncertainty can be assessed based on the unthresholded image I_t. The values which are close to zero or one in I_t are highly certain. The uncertainty can be estimated as $U = |I_t - I_r|$. The uncertainty map for the CCM model with $R = 2\%$ and $n = 21$ is depicted in Fig. 9. As expected, the estimations are highly uncertain near the image edges: the algorithm needs many more samples to determine the exact location of the edges. However, estimations made far from edges are highly certain.

To illustrate the effectiveness of the proposed modeling scheme, another experiment is arranged by comparing our results with ordinary DS (Mariethoz et al., 2010) for $R = 3\%$. This is done by allowing DS to use all the training patterns of the complete TI of Fig. 10(a) as its model. DS achieves the reconstruction accuracy of 92.25 in this scenario (Fig. 10(b)).

SIMPAT is also a patch-based simulation algorithm with promising results (Arpat and Caers, 2007). Fig. 10(c) shows the output of SIMPAT for $R = 3\%$ using the TI of Fig. 10(a). The reconstruction accuracy is 90.13 in this case. Interestingly, the best result of our algorithm obtained using CCM shows an accuracy of 92.48, which is slightly better than DS and SIMPAT (Fig. 7(d)). In other words, the simple and general model proposed in this paper presents results comparable or even better than the results produced using the appropriate training image of Fig. 10(a).

It should be emphasized that although the TI-based methods produce results comparable to the newly developed algorithm, they are sensitive to the selected TI. This can be demonstrated by using an inadequate TI which is not a good representative for the field of interest. Fig. 10(d) and (e) shows the results of DS and SIMPAT for $R = 3\%$ using the inadequate TI of Fig. 1(b). The reconstruction accuracy of TI-based methods is significantly decreased when using a wrong TI.

The algorithm is also tested on the binary image of Fig. 1(b) and the results are depicted in Figs. 11 and 12. Here, no constraint is applied to our models and the algorithm is implemented using only ULEM and UCM. The patch sizes are considered as 19×19 and 21×21 for ULEM and UCM respectively. Because of the specific structure of the image, UCM does not provide meaningful improvement compared to ULEM. Again, the proposed algorithm significantly outperforms the DS method, especially for lower sampling rates.

The tests are repeated for the more complex image of Fig. 1 (c) and the results are depicted in Figs. 13 and 14. Here, the patch sizes are considered as 13×13 and 17×17 for ULEM and UCM respectively. It should be emphasized that the results presented are not the best results achievable using the proposed approach. As illustrated in supplementary materials, by changing the patch size, slightly higher reconstruction accuracies are also achievable.

6.1. Sensitivity to the patch size

The proposed algorithm is sensitive to the patch size to some extent. Fig. 15(a), (b), and (c) illustrates the reconstruction accuracy of our algorithm for the channelized image of Fig. 1(a) for different sampling rates and different window sizes using ULEM, UCM, and CCM respectively. Several different results can be inferred from these plots. Firstly, the plots show that the proper patch size is a function of sampling rate: for lower sampling rates it is reasonable to employ larger patches. The patch should also be sufficiently large to include enough samples to be used in gradient-descent optimization.

Secondly, the combinatorial models present their best results with larger patch sizes compared to ULEM. The higher flexibility of combinatorial models enables them to handle the variability of larger patches. It should be noted that the proper patch size depends on the field behavior as well. Thirdly, UCM provides more stable results compared to the other two models. For different sampling rates, UCM presents equivalently good results for all

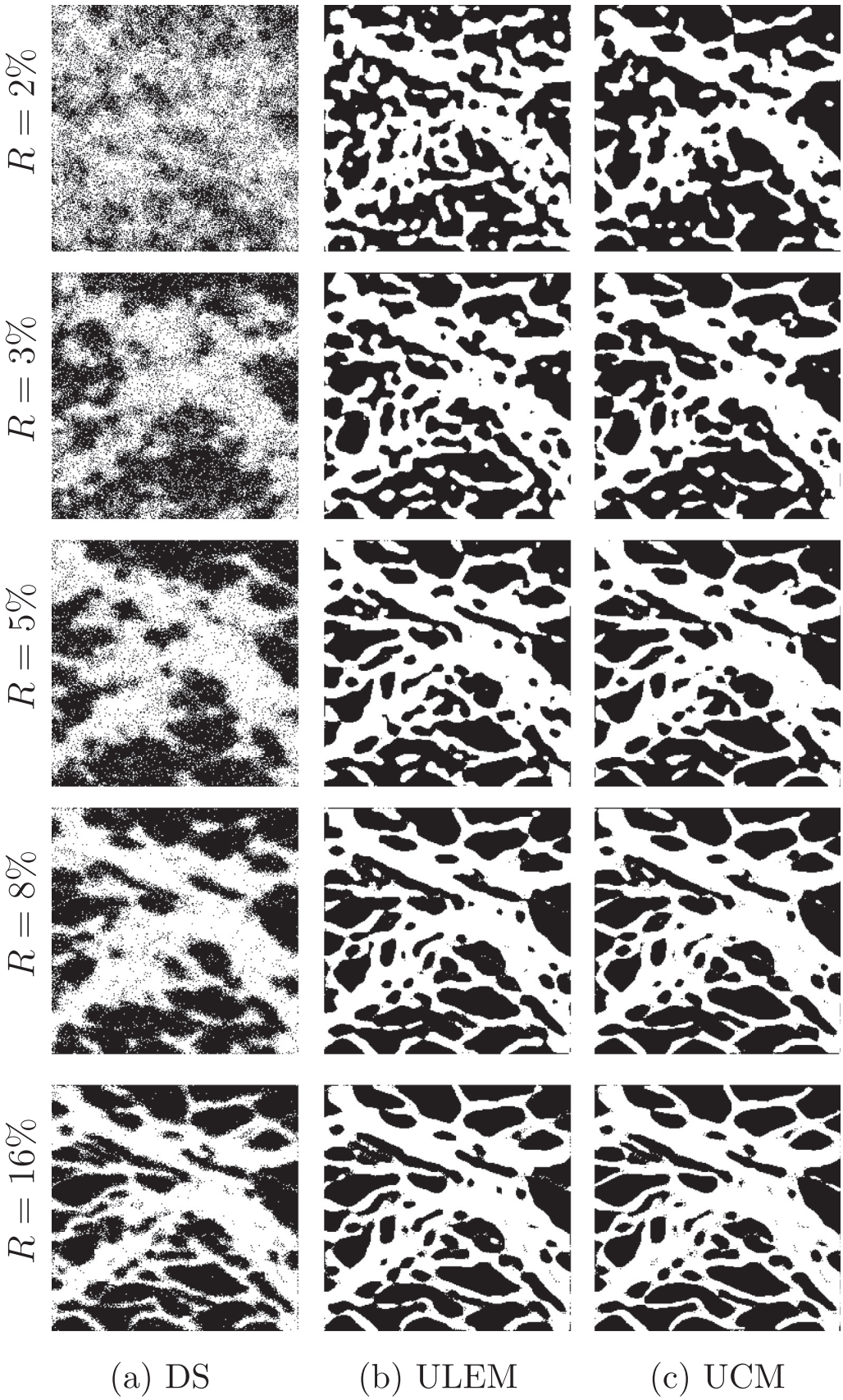

Fig. 13. Reconstruction of incomplete images sampled at different rates R=2%, 3%, 5%, 8% and 16% using DS (Mariethoz and Renard, 2010) and the proposed method with models ULEM and UCM. The tests are performed on randomly distributed samples extracted from Fig. 1(c).

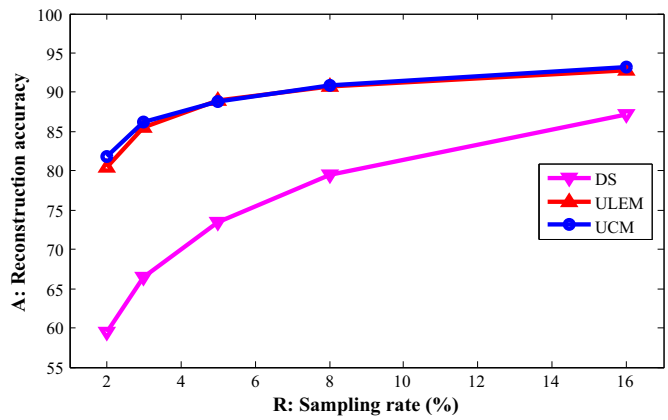

Fig. 14. Reconstruction accuracies for images depicted in Fig. 13.

$n \geq 13$. This could also be justified by higher flexibility of UCM which enables it to perform well for different patch sizes. On the other hand, CCM provides relatively poor results for $n \leq 13$ because it is difficult to enforce a channel width of 8 pixels with such small patches.

Fig. 15 (a) shows that the ULEM performance decreases by increasing the patch size beyond a certain value. This can be justified by the limited variability of the ULEM model for modeling large patterns.

6.2. Algorithm performance

The algorithm performance is also assessed using the image shown in Fig. 1(a). All experiments are carried out in MATLAB environment on a laptop computer with a 2.6 GHz processor. The CPU-time depends on the patch size, the sampling rate, and the selected model. The sampling rate also affects the CPU-time of DS. For comparing the performances, the DS parameters are fixed to $n_{DS} = 50$, $r = 20$, and $f = 1$. Then, the CPU-time of DS is compared with the proposed method for different patch-sizes, different sampling rates and different models. In Fig. 16, $G = \frac{t(DS)}{t(OA)}$ is plotted versus patch size, where $t(DS)$ and $t(OA)$ denote the CPU-time of DS and our algorithm respectively. The plots show that the proposed algorithm performs faster than DS by a factor ranging from 6 to 660. In a special case, using ULEM model the algorithm performs 117 times faster than DS for $R = 16\%$ and $n = 13$. DS takes 7384 s in this test, while our algorithm requires only 63 s.

7. Conclusion

An optimization-based image reconstruction method is proposed in this paper. The heart of the proposed method consists of an analytical model for image patches. The basic assumption of the model is that the image patches can be modeled using either a linear edge or a combination of two linear edges. Finding a match for a given image patch in the model space is formulated using efficient gradient-descent optimization. This leads to a significant speed-up compared to training-image based approaches which work based on exhaustive search.

The proposed method has some advantages and drawbacks. The method presents promising results for randomly distributed data representing more than 1% of the image. As the main advantage, the method does not require any training image. For high sampling rates where the conditional data reflects the geological pattern, the results are comparable to the results of TI-based methods (e.g. DS and SIMPAT) when using adequate TIs and far better than them when using wrong TIs. As expected, in the absence of a TI or any other geostatistical model, the proposed method cannot provide acceptable results for low sampling rates (lower than 1%) where the conditional data does not reflect the geological pattern. Furthermore the method is incapable of reconstructing images with samples concentrated in a limited region leaving the remainder of the image empty.

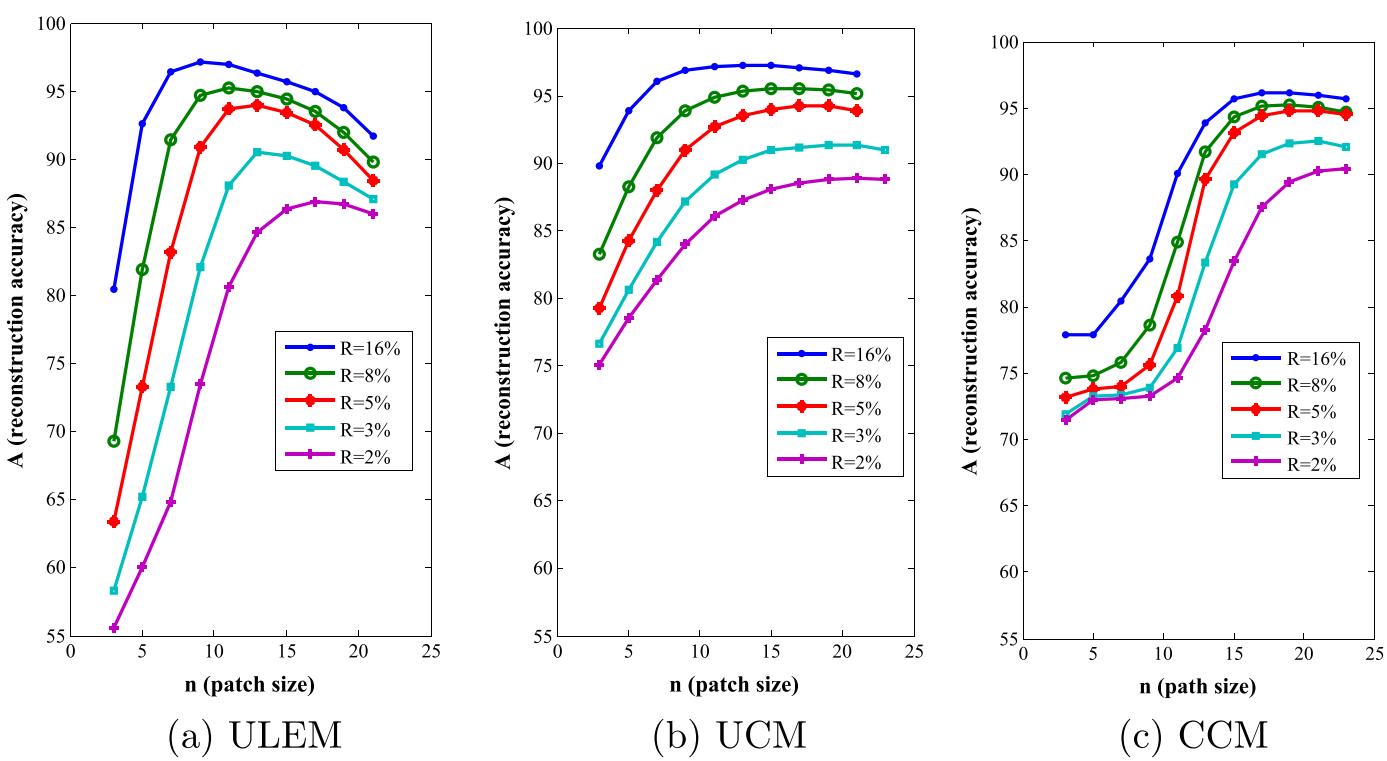

Fig. 15. Sensitivity of the proposed method to the patch size (n) for different sampling rates and different models ULEM, UCM, and CCM.

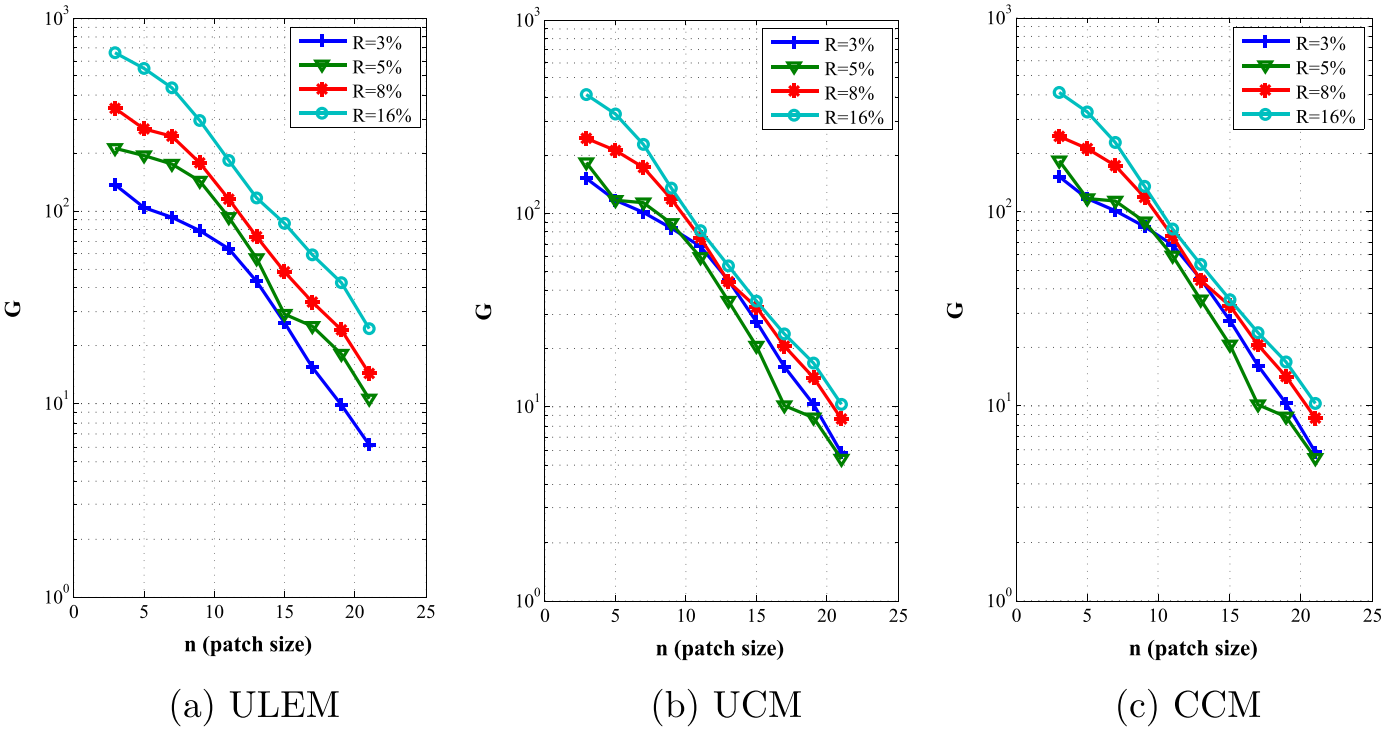

Fig. 16. Comparison of CPU-time of the proposed method with DS for different patch sizes, different sampling rates and different models ULEM, UCM, and CCM. $G = \frac{t(DS)}{t(OA)}$. The DS parameters are fixed to $n_{DS} = 50$, $r = 20$, $f = 1$ in all tests.

Acknowledgments

The authors would like to express their thanks to Gregoire Mariethoz and two anonymous reviewers for their constructive comments on the paper.

Appendix A. Supplementary data

Supplementary data associated with this paper can be found in the online version at http://dx.doi.org/10.1016/j.cageo.2015.12.018.

References

Abdollahifard, M.J., 2016. Fast multiple-point simulation using a data-driven path and an efficient gradient-based search. Comput. Geosci. 86, 64–74.
Abdollahifard, M.J., Faez, K., 2013a. Fast direct sampling for multiple-point stochastic simulation. Arab. J. Geosci., 1–13.
Abdollahifard, M.J., Faez, K., 2013b. Stochastic simulation of patterns using bayesian pattern modeling. Comput. Geosci. 17, 99–116.
Allard, D., Froidevaux, R., Biver, P., 2005. Accounting for non-stationarity and interactions in object simulation for reservoir heterogeneity characterization. In: Geostatistics Banff 2004. Springer, pp. 155–164.
de Almeida, J.A., 2010. Stochastic simulation methods for characterization of lithoclasses in carbonate reservoirs. Earth-Sci. Rev. 101, 250–270.
Arpat, G.B., Caers, J., 2007. Conditional simulation with patterns. Math. Geol. 39, 177–203.
Bárdossy, A., Li, J., 2008. Geostatistical interpolation using copulas. Water Resour. Res. 44.
Bastante, F., Ordóñez, C., Taboada, J., Matías, J., 2008. Comparison of indicator Kriging, conditional indicator simulation and multiple-point statistics used to model slate deposits. Eng. Geol. 98, 50–59.
Bishop, C.M., 2006. Pattern Recognition and Machine Learning. Springer.
Calderon, H., Silva, J.F., Ortiz, J.M., Egaña, A., 2015. Reconstruction of channelized geological facies based on ripless compressed sensing. Comput. Geosci. 77, 54–65.
Chu, L., Reynolds, A., Oliver, D.S., 1995. Reservoir description from static and well-test data using efficient gradient methods. In: International Meeting on Petroleum Engineering, pp. 467–482.
Deutsch, C., Tran, T., 2002. Fluvsim: a program for object-based stochastic modeling of fluvial depositional systems. Comput. Geosci. 28, 525–535.
Dimitrakopoulos, R., Mustapha, H., Gloaguen, E., 2010. High-order statistics of spatial random fields: exploring spatial cumulants for modeling complex non-Gaussian and non-linear phenomena. Math. Geosci. 42, 65–99.
Emery, X., 2007. Using the Gibbs sampler for conditional simulation of gaussian-based random fields. Comput. Geosci. 33, 522–537.
Feyen, L., Caers, J., 2006. Quantifying geological uncertainty for flow and transport modeling in multi-modal heterogeneous formations. Adv. Water Resour. 29, 912–929.
Green, C.T., Böhlke, J.K., Bekins, B.A., Phillips, S.P., 2010. Mixing effects on apparent reaction rates and isotope fractionation during denitrification in a heterogeneous aquifer. Water Resour. Res. 46.
Honarkhah, M., Caers, J., 2010. Stochastic simulation of patterns using distance-based pattern modeling. Math. Geosci. 42, 487–517.
Keogh, K.J., Martinius, A.W., Osland, R., 2007. The development of fluvial stochastic modelling in the Norwegian oil industry: a historical review, subsurface implementation and future directions. Sediment. Geol. 202, 249–268.
Klise, K.A., Weissmann, G.S., McKenna, S.A., Nichols, E.M., Frechette, J.D., Wawrzyniec, T.F., Tidwell, V.C., 2009. Exploring solute transport and streamline connectivity using lidar-based outcrop images and geostatistical representations of heterogeneity. Water Resour. Res. 45.
Knudby, C., Carrera, J., 2005. On the relationship between indicators of geostatistical, flow and transport connectivity. Adv. Water Resour. 28, 405–421.
Lantuéjoul, C., 2002. Geostatistical Simulation: Models and Algorithms, vol. 1139. Springer Science & Business Media.
Lee, T.Y., Seinfeld, J.H., 1987. Estimation of two-phase petroleum reservoir properties by regularization. J. Comput. Phys. 69, 397–419.
Li, R., Reynolds, A., Oliver, D.S., et al., 2003. History matching of three-phase flow production data. SPE J. 8, 328–340.
Mariethoz, G., Caers, J., 2014. Multiple-Point Geostatistics: Stochastic Modeling with Training Images. Wiley-Blackwell.
Mariethoz, G., Kelly, B.F., 2011. Modeling complex geological structures with elementary training images and transform-invariant distances. Water Resour. Res. 47.
Mariethoz, G., Renard, P., 2010. Reconstruction of incomplete data sets or images using direct sampling. Math. Geosci. 42, 245–268.
Mariethoz, G., Renard, P., Cornaton, F., Jaquet, O., 2009. Truncated plurigaussian simulations to characterize aquifer heterogeneity. Groundwater 47, 13–24.
Mariethoz, G., Renard, P., Straubhaar, J., 2010. The direct sampling method to perform multiple-point geostatistical simulations. Water Resour. Res. 46.
Michael, H., Li, H., Boucher, A., Sun, T., Caers, J., Gorelick, S., 2010. Combining geologic-process models and geostatistics for conditional simulation of 3-d subsurface heterogeneity. Water Resour. Res. 46.
Peyré, G., 2009. Manifold models for signals and images. Comput. Vis. Image Underst. 113, 249–260.
Pyrcz, M., Boisvert, J.B., Deutsch, C.V., 2009. Alluvsim: a program for event-based stochastic modeling of fluvial depositional systems. Comput. Geosci. 35, 1671–1685.

Pyrcz, M.J., Boisvert, J.B., Deutsch, C.V., 2008. A library of training images for fluvial and deepwater reservoirs and associated code. Comput. Geosci. 34, 542–560.
Straubhaar, J., Renard, P., Mariethoz, G., Froidevaux, R., Besson, O., 2011. An improved parallel multiple-point algorithm using a list approach. Math. Geosci. 43, 305–328.
Strebelle, S., 2002. Conditional simulation of complex geological structures using multiple-point statistics. Math. Geol. 34, 1–21.
Suzuki, S., Caers, J., 2008. A distance-based prior model parameterization for constraining solutions of spatial inverse problems. Math. Geosci. 40, 445–469.
Western, A.W., Blöschl, G., Grayson, R.B., 2001. Toward capturing hydrologically significant connectivity in spatial patterns. Water Resour. Res. 37, 83–97.
Zhang, T., Switzer, P., Journel, A., 2006. Filter-based classification of training image patterns for spatial simulation. Math. Geol. 38, 63–80.